Research Article Wiley Online Library ELECTROANALYSIS

doi.org/10.1002/elan.202100080

An Enzyme-free Electrochemical H_2O_2 Sensor Based on a Nickel Metal-organic Framework Nanosheet Array

Xiao Liu,[a] Mei-Hao Xiang,[a] Xinyue Zhang,[a] Qin Li,[a] Xiaoya Liu,[a] Wenjing Zhang,[a] Xia Qin,*[b] and Fengli Qu*[a]

Abstract: In this work, we reported the development of a nickel metal-organic framework nanosheet array on Ti-mesh (Ni-MOF/TM) as an enzyme-free electrochemical sensing platform for H_2O_2 determination. The as-obtained sensor exhibited outstanding detection properties of H_2O_2, which might be gifted from the large specific surface area, abundant active sites of Ni-MOF nanoarrays. The sensor displayed a good linear range (0.8 μM–4.6 × 10^3 μM), a detection limit as low as 0.26 μM, a high sensitivity (307.5 μA mM^{-1} cm^{-2}), and a rapid response. Moreover, this enzyme-free sensor is promising for point-of-care (POC) testing of H_2O_2 in human serum attribute to the excellent performance of Ni-MOF and the simple preparation process of the sensor.

Keywords: Electrochemical · Hydrogen peroxide · Ni-MOF · Point of care (POC) testing

1 Introduction

Hydrogen peroxide (H_2O_2), a common peroxide, plays a significant role in biological systems, medical diagnosis, environmental analyses, food, industrial, and many other fields [1–3]. Besides, H_2O_2 as a crucial member of reactive oxygen species (ROS) that are closely related to life activities of biology [4]. The excessive level of H_2O_2 can cause a series of diseases such as Alzheimer's, Parkinson's, myocardial infarction, inflammatory lung diseases, and cancer, etc [5,6]. Therefore, developing an effective method for measuring H_2O_2 levels quickly and accurately is essential [7,8].

Current analytical methods for detecting H_2O_2 involve ELISA, cell imaging, high-performance liquid chromatography (HPLC), fluorescence detection, etc [9–12]. However, all mentioned detection platforms require complex and relatively expensive instruments. By contrast, point-of-care (POC) testing is time-efficient, low-cost, and easy to use [13]. The electrochemical sensor stands out for wide developments toward point-of-care testing in virtue of its advantages of rapidness, low cost, simplicity, and sensitive detection system. So electrochemical sensor is a promising method for POC testing of H_2O_2 [14]. In earlier research, enzyme-based sensors for detecting H_2O_2 have received extensively studies, owing to their great sensitivity and high selectivity. Nevertheless, their wide application is largely hindered by high-cost, complex enzyme immobilization processes, and inherent instability of natural enzymes [15]. To overcome these challenges, more and more investigations have been concentrated on development of superior enzyme-free H_2O_2 sensors, which possess high sensitivity, low budgets, the simple preparation process as well as long-term stability [14–17]. Although noble metals, carbon materials, and transition metal oxides, etc. as active materials in enzyme-free sensing systems show great electrochemical properties, their applications were restricted by high cost, poor electrical conductivity, and these metals easily poisoned by the adsorbed intermediates [18]. Thus, it is highly desirable to explore advanced materials for the enzyme-free electrochemical sensor for the POC testing of H_2O_2.

Metal-organic frameworks (MOFs) have raised concerns about the features of adjustable and ordered porous structures, high specific surface area, exposed metal sites, and adsorption affinities [19–21]. These superior performances make MOFs as ideal material for gas storage, separation, drug delivery and biosensing [22–24]. However, poor conductivity and stability of MOFs, which limits their electrochemical applications in the biosensor analysis [25]. Recently, the design and synthesis of new MOFs with redox metal cations (Ni-, Zr-, Co-, Fe-, and Zn), especially that of nickel-based MOFs (Ni-MOFs) with superb conductivity provide an effective way to overcome the above disadvantages. For example, Zhang et al. successfully synthesized simple Ni-MOFs and found that the obtained Ni-MOF nanostructures can enhance the electron transfer, as well as facilitate close contact between glucose and catalytic sites [26]. Du et al. also reported that their obtained hierarchical porous Ni-MOFs could provide more electroactive sites for electrochemical

[a] X. Liu, M.-H. Xiang, X. Zhang, Q. Li, X. Liu, W. Zhang, F. Qu
College of Chemistry and Chemical Engineering, Qufu Normal University, Qufu 273165, Shandong, China
E-mail: xiaqin_2009@163.com
[b] X. Qin
School of Geography and Tourism, Qufu Normal University, Rizhao 276826, Shandong, China
E-mail: fengliquhn@hotmail.com

Supporting information for this article is available on the WWW under https://doi.org/10.1002/elan.202100080

reactions because of the larger specific surface area [27]. Qiao's group reported the conductive Ni-MOFs could act as a low-cost catalyst for non-enzymatic determination of glucose with excellent electrochemical properties [28]. According to these characteristics of Ni-MOFs, it can be envisaged that the Ni-MOFs can be used as an outstanding electrocatalyst for the enzyme-free sensing of H_2O_2.

Herein, an enzyme-free electrochemical H_2O_2 sensor based on a Ni-MOF nanosheet array was reported. The proposed biosensor for the reduction of H_2O_2 was fabricated via in-situ growing Ni-MOF onto the Ti mesh (Ni-MOF/TM) (Scheme 1). Firstly, the Ni-MOF nanoarrays structure can promote the electrochemical property of materials by increasing the electrocatalytic active sites and enhancing the conductivity [28]. Secondly, abundant unsaturated metal sites of Ni^{2+} can furnish catalytic active center [29]. Last but not least, the porous structure and high specific surface area increases the area of ion contact [30]. Under optimal conditions, the proposed Ni-MOF/TM electrochemical sensor exhibited high sensitivity and selectivity toward H_2O_2 with a low detection limit of 0.26 μM. Owing to the above remarkable analytical advantages, the Ni-MOF/TM has great potential in the point-of-care (POC) testing of H_2O_2 in human serum.

2 Experimental Section

2.1 Reagents and Materials

$Ni(NO_3)_2 \cdot 6H_2O$, C_2H_5OH, H_2O_2 (30 wt %), Na_2HPO_4, NaH_2PO_4, N, N-Dimethylformamide (DMF), NaCl were acquired from Sinopharm Chemical Reagent Co., Ltd. Terephthalic acid ($C_8H_4O_4$), uric acid (UA), dopamine (DA), ascorbic acid (AA), glucose (Glu), and sucrose (Suc) were bought from Aladdin Ltd. (Shanghai, China). All reagents were used as received.

2.2 Fabrication of Ni-MOF/TM Sensor

Ni-MOF nanosheets were synthesized based on previous work [21]. Firstly, a piece of Ti mesh (TM, 2 cm × 3 cm) was pretreated by hydrochloric acid, ethanol and deionized water before use. Then, 35 mL of N,N-dimethylformamide (DMF) solution containing 2.36 mmol $Ni(NO_3)_2 \cdot 6H_2O$ and 1.75 mmol terephthalic acids was vigorously stirred to obtain a clarification solution. Following, the above solution was mixed with 2.5 mL H_2O and 2.5 mL ethanol and stirred for 40 min. The mixture was then transferred to a Teflon-lined stainless-steel autoclave with TM, which was allowed to react for 12 h at 120 °C. Then, the TM was washed several times with ethanol and ultrapure water. Eventually, the obtained electrode was dried for 3 hours.

2.3 Instrumentation

Electrochemical experiments were performed in a standard three electrode system using a CHI 660E electrochemical workstation (CH Instruments, Inc., Shanghai)). Ni-MOF/TM (0.2 cm × 0.2 cm), Ag/AgCl, and graphite as the working electrode, reference electrode and counter electrode, respectively. X-ray diffraction (XRD) patterns were determined utilizing MiniFlex600 (Rjgaku Co. Japan) with Cu Kα radiation (λ = 1.5406 Å). Scanning electron microscopy (SEM) image was acquired on SU3500 scanning electron microscope (HITACHI, Japan) at an accelerating voltage of 2 kV. Transmission electron microscopy (TEM) image was recorded with HITACHI H-8100 electron microscopy (Hitachi, Japan) operating at 200 kV. X-ray photoelectron spectroscopy (XPS) was measured with Thermo ESCALAB 250Xi, by use of Mg X-ray source.

3 Results and Discussion

3.1 Characterization

The compositions and phase of Ni-MOF/TM were analyzed by X-ray diffraction (XRD) (Figure 1a). There were two sharp peaks at 8.6° and 16.9°, which could be assigned to the (100) and (200) planes of $Ni_3(OH)_2(C_8H_4O_2)_2(H_2O)_4$ (CCDC No. 638866), respectively [31,32], indicating the successful synthesis of the materials. The scanning electron microscopy (SEM) image of Ni-MOF/TM (Figure 1b) revealed that the Ni-MOF presented a typical sheet-like array structure. Furthermore, TEM analysis was applied to investigate the single nanosheet morphology (Figure 1c), suggesting the Ni-MOF obtained by the ultrasonic treatment displayed an ultrathin nanosheet structure with a transparent morphology. Moreover, Figure S1 displayed the energy

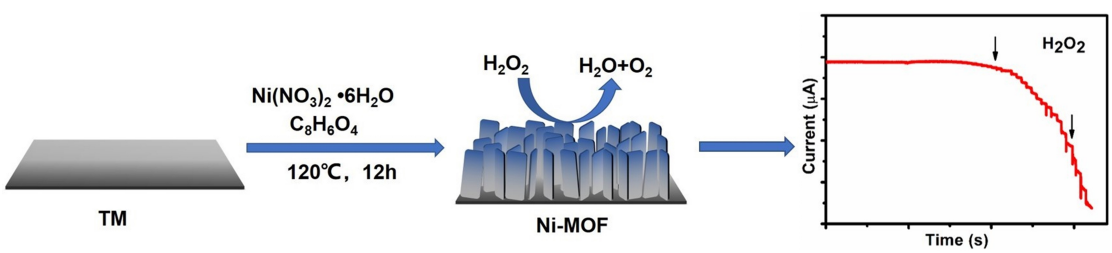

Scheme 1. Schematic diagram for the preparation of Ni-MOF nanoarrays.

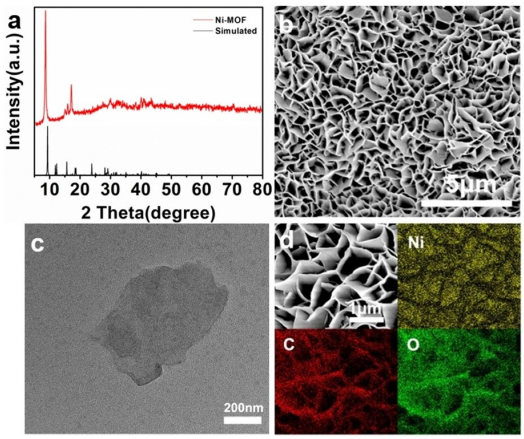

Fig. 1. (a) XRD patterns (b) SEM image of Ni-MOF/TM. (c) TEM image of Ni-MOF nanosheet. (d) EDS mapping images of Ni-MOF/TM.

dispersive X-ray (EDS) spectrum of Ni-MOF/TM, which demonstrated the presence of Ni, C, and O elements with an atomic ratio of 0.10:0.41:0.49, and EDS mapping images further verified the Ni, C, and O elements distributed over the whole nanoarrays (Figure 1d).

As plotted in Figure 2a, the XPS survey spectrum was utilized to identify the chemical composition of Ni-MOF/TM. There were three strong peaks at 278.96 (C 1s), 528.14 (O 1s), and 857.69 eV (Ni 2p), which proved the coexistence of Ni, C and O elements [24]. In Figure 2b, the major peaks positioned at 857.2 and 875.3 eV were assigned to Ni $2p_{3/2}$ and Ni $2p_{1/2}$ states, respectively [33], and the satellites peaks at 862.8 and 881.0 eV were the Ni shakeup type peaks [34]. Figure 2c exhibits the C 1s region, the XPS peaks at 284.3, 286.1 and 289.3 eV belong to C=C, C–O and O-C=O bonds of terephthalate, respectively [35,36]. The XPS spectrum of O 1s (Figure 2d) was divided into two peaks, corresponding to the metal-oxygen bond (M–O) at a binding energy of 531.0 eV and the OH group at a binding energy of

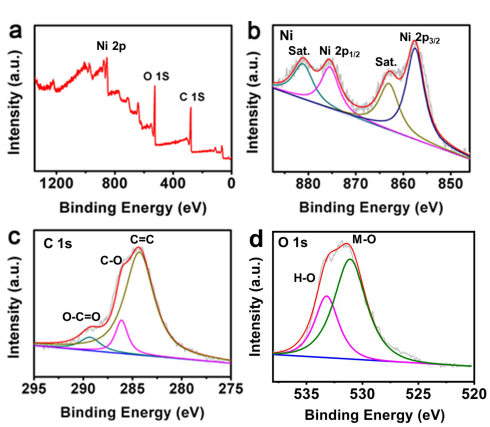

Fig. 2. (a) XPS spectra of Ni-MOF/TM. (b) Ni 2p, (c) C 1s and (d) O 1s XPS spectra of Ni-MOF/TM.

533.1 eV [37]. The observations described above indicate that the preparation of the material is successful. The Brunauer-Emmett-Teller (BET) surface area of the Ni-MOF was obtained from the N_2 adsorption/desorption measurement. The results showed that the BET surface area was 55.0091 m^2/g, this specific surface area and the porous structure is sufficient to increase the ionic contact surface (Figure S2).

3.2 Electrochemical Property of Biosensor for H_2O_2 Detection

To analyze the performance of the biosensor, the electrochemical responses of the obtained electrode were investigated by a typical three electrode device. Firstly, we measured the CV response of bare TM and Ni-MOF/TM in 5 mM $[Fe(CN)_6]^{3-/4-}$ solution (Figure S3). In contrast to bare TM, the Ni-MOF/TM brought evidently enhanced CV response. After that, the property of the biosensor for detecting H_2O_2 was studied in 0.1 M PBS. In Figure 3a, no obvious reduction peak was observed on bare TM (curves a and b) without or with 9 mM H_2O_2, suggesting that the detection of H_2O_2 by bare TM electrodes is electrochemical inert. By contrast, under identical experimental conditions, the reduction peak on Ni-MOF/TM (curves c and d) increased significantly after the addition of H_2O_2, which verified the feasibility of the proposed sensor. In Figure 3b, As the concentration of H_2O_2 increased from 0 to 9 mM, the CVs responses correspondingly enhanced, which demonstrated the excellent sensing property of biosensor towards H_2O_2. According to the report, the electrocatalytic mechanism was explained as follows [38]:

$$\text{Ni-MOF (Ox)} + e^- \rightleftharpoons \text{Ni-MOF (Red)} \quad (1)$$

$$\text{Ni-MOF (Red)} + 2H_2O_2 \rightleftharpoons \text{Ni-MOF (Ox)} + 2H_2O + O_2 \quad (2)$$

As plotted in Figure 3c, for the scan rates within 20–200 $mV\,s^{-1}$, both the anodic and cathodic peak currents enhanced significantly. Moreover, the densities of anode current and cathode current were proportional to the scan rate (Figure 3d), revealing a typical absorption control mechanism [39]. To acquire the most appropriate reduction potential for electrochemical detection of H_2O_2, the amperometric responses of the biosensor towards H_2O_2 under three different potentials (−0.2, −0.3, and −0.4 V) were studied with the successive addition of 1 mM H_2O_2 (Figure S4). In the light of current-time (i–t) measurements, the subsequent tests chose −0.3 V as an optimal potential due to the suitable current response and signal-to-noise ratio. Then, the current response of Ni-MOF/TM for H_2O_2 sensing was monitored by continuously adding H_2O_2 at −0.3 V to evaluate the detection sensitivity of the sensor. The recorded current on Ni-MOF/TM steadily increased with the successive injection of H_2O_2 and achieved steady state within 3 s (Figure 4a). As being

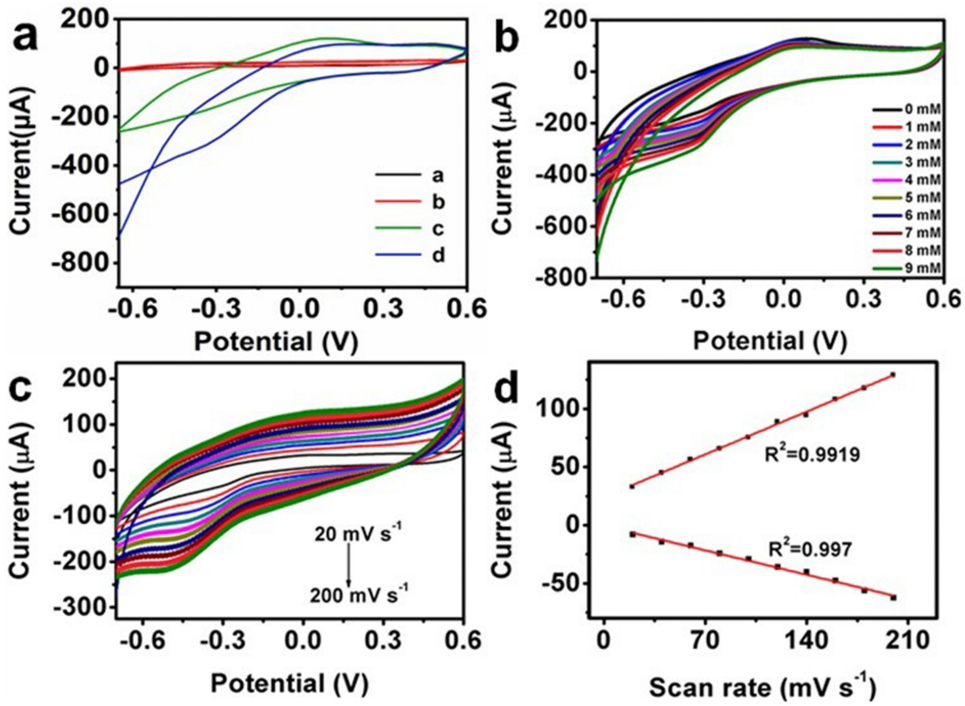

Fig. 3. (a) The cyclic voltammograms of bare Ti mesh (curves a and b) and Ni-MOF/TM (curves c and d) in 0.1 M PBS (pH = 7.4) without or with 9 mM H_2O_2. (b) CVs of Ni-MOF/TM in 0.1 M PBS with different H_2O_2 concentrations at 50 mV s^{-1}. (c) CVs of 1 mM H_2O_2 in 0.1 M PBS on Ni-MOF/TM at diverse scan rates (20–200 mV s^{-1}). (d) The calibrated diagram of the peak currents versus scan rates.

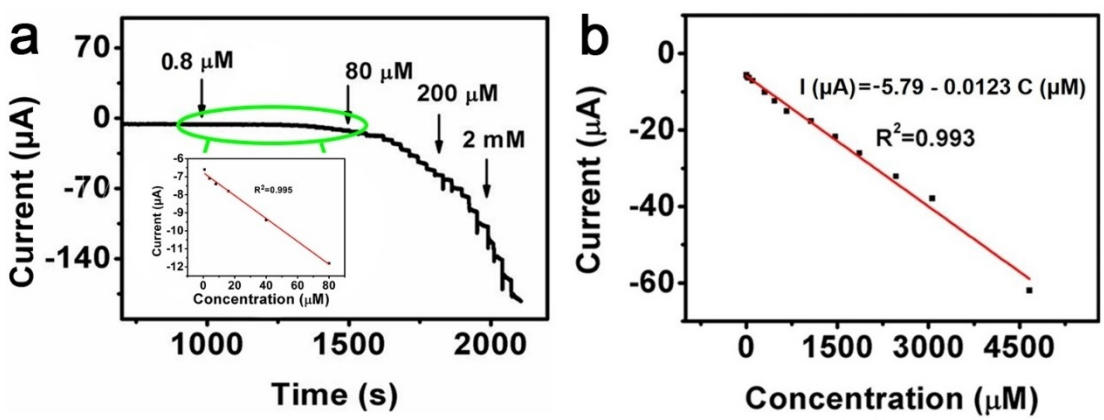

Fig. 4. (a) The amperometric current-time curves of Ni-MOF/TM with the continuous injection of H_2O_2 in 0.1 M PBS. The inset shows the calibration plot of current response versus low H_2O_2 concentrations. (b) The calibration plot for H_2O_2 detection.

plotted in Figure 4b, the linear detection ranges from 0.8 to 4.6×10^3 μM was obtained from the Ni-MOF/TM, and the regression equation could be described as I (μA) = −5.79 - 0.0123 C (μM) ($R^2 = 0.9932$). Moreover, the calculated limit of detection was 0.26 μM (S/N = 3) and high-sensitivity of 307.5 μA mM^{-1} cm^{-2}. These results indicated that the biosensor proposed here outperforms other electrochemical H_2O_2 sensors reported previously (Table 1). The superior performance of the H_2O_2 sensor can be ascribed to the advantages of Ni-MOF described below: (1) the Ni-MOF nanoarrays provide a large number of electrocatalytic active sites for the adsorption and reduction of H_2O_2. (2) porous structure increases the area of ion contact, which enables faster electron transfer and facilitates the reduction of H_2O_2.

In practical application, selectivity and stability are the main factors affecting analytical performance. The selectivity of Ni-MOF/TM was evaluated by adding various possible interfering reagents, such as ascorbic acid (AA), dopamine (DA), glucose (Glu), NaCl, sucrose (Suc), and Urea, coexisting with H_2O_2 in physiological conditions. As plotted in Figure 5, except for the significant current

Table 1. Compare the performance of the proposed biosensor with other reported sensors for H_2O_2 detection.

Sensor	Sensitivity ($\mu A\,mM^{-1}\,cm^{-2}$)	Linear range (μM^{-1})	Detection Limit (μM)	Reference
(Ag/PNA)/CPE	36.8777	1–3000	0.9247	[40]
n-CoZnE	13.3	0.1–2400	11.1	[41]
CuO/g-C_3N_4/GCE	–	0.5–50	0.31	[42]
SnS_2/Pt NPs	36.57	1–185	0.33	[43]
AuCu/SPCE	133.74	50–10000	10.93	[44]
2D Cu-TCPP/MWCNTs	157	1–8159	0.7	[45]
Gox/CoS-MWCNTs	15	8–1500	5	[46]
ZIF-67/rGO/GCE	51.86	5–2150	1.5	[47]
Fe_2NiMIL-88B/GCE	124.7	1.2–1800	0.4	[48]
Ni-MOF/TM	307.5	0.8–4600	0.26	This work

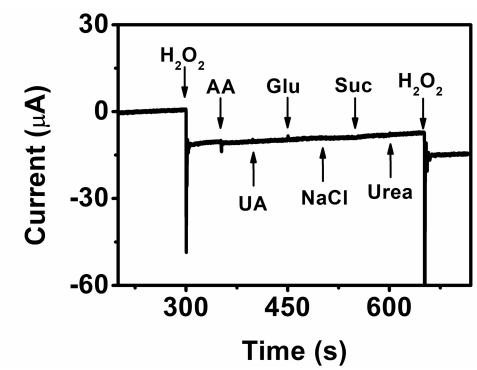

Fig. 5. Chronoamperometric curves of Ni-MOF/TM in 0.1 M PBS with the successive injection of 1 mM H_2O_2, AA, UA, Glu, NaCl, Suc, and Urea. Applied potential: −0.3 V.

response to H_2O_2, none of the above interferences produces remarkable current change, and then, with another addition of H_2O_2, the current response increased sharply again, indicating high selectivity of Ni-MOF/TM towards H_2O_2.

To evaluate the stability of the proposed sensor, we recorded continuous CV responses of 1 mM H_2O_2 20 times (Figure S5). During multiple cycles, the current had no obvious reduction. Moreover, we studied the reproducibility of the proposed sensor for H_2O_2 detection. We investigated the amperometric response of five electrodes under the same optimized condition, and the relative standard deviation (RSD) was found to be 2.8 % (Figure S6). These results suggested satisfactory stability and reproducibility of the sensor.

3.3 Measurement of H_2O_2 in Real Sample

The feasibility of Ni-MOF/TM sensor in real sample was estimated via the recovery measurements in human serum samples, which was obtained from the Qufu Normal University Hospital. The N_2-saturated serum samples and the known concentration of H_2O_2 were spiked into PBS buffer. Based on the results summarized in Table 2, the good recoveries were between 96.7 % and 99.3 %, which indicated the biosensor based on the Ni-MOF/TM could offer potential application for POC testing of H_2O_2 in real samples.

Table 2. Analysis of human serum samples via the obtained biosensor.

Sample	Found (μM)	Added (μM)	Total Found (μM)	RSD (%)	Recovery (%)
Serum 1	12.67	0	12.67	1.8	–
	12.67	10	22.34	1.6	96.7
	12.67	20	32.24	1.7	97.9
	12.67	30	42.46	1.9	99.3
Serum 2	15.52	0	15.52	2.3	–
	15.52	10	25.37	2.0	98.5
	15.52	20	35.02	1.9	97.5
	15.52	30	45.23	2.4	99.0

4 Conclusion

In summary, we reported a Ni-MOF/TM nanosheet array via in-situ growing the Ni-MOF on TM to construct an electrochemical sensor of H_2O_2. The obtained highly reaction sites of Ni-MOF with large specific surface areas, which exhibited excellent catalytic ability for H_2O_2 reduction. The result proved that the proposed sensor was suitable for quantitative H_2O_2 detection with a low detection limit, good selectivity and stability. Moreover, the Ni-MOF nanoarray achieved fast responses at low-potential detection (−0.3 V) and reached steady within 3 s. More importantly, the Ni-MOF nanoarrays displayed potential applications in the H_2O_2 detection in serum. This study opened a new avenue for point-of-care (POC) testing of H_2O_2.

Acknowledgements

We gratefully acknowledge the support of the National Natural Science Foundation of China (22074080, 21775089), Changjiang Scholar Program of the Ministry of Education of China, Taishan scholar of Shandong Province (tsqn201909106), and Project of Shandong Province Higher Educational Science and Technology Program (J18KA101).

Data Availability Statement

Data provided at the author's request.

References

[1] J. Bai, X. Jiang, *Anal. Chem.* **2013**, *85*, 8095–8101.
[2] S. G. Rhee, *Science.* **2006**, *312*, 1882–1883.
[3] W. Wu, J. Li, L. Chen, Z. Ma, W. Zhang, Z. Liu, Y. Cheng, L. Du, M. Li, *Anal. Chem.* **2014**, *86*, 9800–9806.
[4] H. Sies, D. P. Jones, *Nat. Rev. Mol. Cell Biol.* **2020**, *21*, 363–383.
[5] T. Hang, S. Xiao, C. Yang, X. Li, C. Guo, G. He, B. Li, C. Yang, H. J. Chen, F. Liu, S. Deng, Y. Zhang, X. Xie, *Sens. Actuators B* **2019**, *289*, 15–23.
[6] Y. Dong, J. Zheng, *Chem. Eng. J.* **2020**, *392*, 123–690.
[7] L. Shang, B. Zeng, F. Zhao, *ACS Appl. Mater. Interfaces.* **2015**, *7*, 122–128.
[8] K. Yang, H. Zhong, Z. P. Cheng, X. R. Li, A. R. Zhang, T. L. Li, Y. J. Zhang, G. Q. Liu, H. Y. Qian, *J. Electroanal. Chem.* **2018**, *814*, 1–6.
[9] A. S. Ivanova, A. D. Merkuleva, S. V. Andreev, K. A. Sakharov, *Food Chem.* **2019**, *283*, 431–436.
[10] X. Zhou, M. Xu, H. Huang, A. Mazar, Z. Iqbal, C. Yuan, M. Huang, *Talanta.* **2016**, *160*, 205–210.
[11] Y. Liu, J. Niu, J. Nie, F. Meng, W. Lin, *New J. Chem.* **2017**, *41*, 3320–3325.
[12] M. C. Chang, A. Pralle, E. Y. Isacoff, C. J. Chang, *J. Am. Chem. Soc.* **2004**, *126*, 15392–15393.
[13] Y. Manmana, T. Kubo, K. Otsuka, *Anal. Chem.* **2021**, *135*, 116160.
[14] Y. Dai, C. C. Liu, *Angew. Chem. Int. Ed.* **2019**, *58*, 12355–12368; *Angew. Chem.* **2019**, *131*, 12483–12496.
[15] F. Xie, X. Cao, F. Qu, A. M. Asiri, X. Sun, *Sens. Actuators B* **2018**, *255*, 1254–1261.
[16] B. Liu, X. Wang, Y. Zhai, Z. Zhang, H. Liu, L. Li, H. Wen, *J. Electroanal. Chem.* **2020**, *858*.
[17] X. Qin, H. Wang, Z. Miao, J. Li, Q. Chen, *Talanta.* **2015**, *139*, 56–61.
[18] H. Du, R. Kong, F. Qu, L. Lu, *Chem. Commun.* **2018**, *54*, 10100–10103.
[19] C. Wang, N. Zhang, D. Wei, R. Feng, D. Fan, L. Hu, Q. Wei, H. Ju, *Biosens. Bioelectron.* **2019**, *142*, 111521.
[20] C. Yang, X. Li, L. Yu, X. Liu, J. Yang, M. Wei, *Chem. Commun.* **2020**, *56*, 1803–1806.
[21] L. Yang, G. Zhu, H. Wen, X. Guan, X. Sun, H. Feng, W. Tian, D. Zheng, X. Cheng, Y. Yao, *J. Mater. Chem. A.* **2019**, *7*, 8771–8776.
[22] L. Chen, W. Yang, X. Li, L. Han, M. Wei, *J. Mater. Chem. A.* **2019**, *7*, 10331–10337.
[23] Q. Yang, Q. Xu, H. L. Jiang, *Chem. Soc. Rev.* **2017**, *46*, 4774–4808.
[24] X. Xiao, S. Zheng, X. Li, G. Zhang, X. Guo, H. Xue, H. Pang, *J. Mater. Chem. B.* **2017**, *5*, 5234–5239.
[25] H. S. Choi, X. Yang, G. Liu, D. S. Kim, J. H. Yang, J. H. Lee, S. O. Han, J. Lee, S. W. Kim, *J. Taiwan Inst. Chem. E.* **2020**, *113*, 1–7.
[26] X. Zhang, Y. Xu, B. Ye, *J. Alloys Compd.* **2018**, *767*, 651–656.
[27] P. Du, Y. Dong, C. Liu, W. Wei, D. Liu, P. Liu, *J. Colloid Interface Sci.* **2018**, *518*, 57–68.
[28] M. Yuan, R. Wang, Z. Sun, L. Lin, H. Yang, H. Li, C. Nan, G. Sun, *J. Mater. Chem. B.* **2019**, *58*, 11449–11457.
[29] Y. Qiao, Q. Liu, S. Lu, G. Chen, S. Gao, W. Lu, X. Sun, *J. Mater. Chem. B.* **2020**, *8*, 5411–5415.
[30] Y. Li, Y. Xu, Y. Liu, H. Pang, *Small.* **2019**, *15*, 1902463.
[31] Q. Liu, L. Xie, X. Shi, G. Du, A. M. Asiri, Y. Luo, X. Sun, *Inorg. Chem. Front.* **2018**, *5*, 1570–1574.
[32] J. Yang, C. Zheng, P. Xiong, Y. Li, M. Wei, *J. Mater. Chem. A.* **2014**, *2*, 19005–19010.
[33] X. Luan, H. Du, Y. Kong, F. Qu, L. Lu, *Chem. Commun.* **2019**, *55*, 7335–7338.
[34] X. Zhu, C. Tang, H. F. Wang, B. Q. Li, Q. Zhang, C. Li, C. Yang, F. Wei, *J. Mater. Chem. A.* **2016**, *4*, 7245–7250.
[35] Q. Cheng, K. Tao, X. Han, Y. Yang, Z. Yang, Q. Ma, L. Han, *Dalton Trans.* **2019**, *48*, 4119–4123.
[36] Q. Chen, S. Lei, P. Deng, X. Ou, L. Chen, W. Wang, Y. Xiao, B. Cheng, *J. Mater. Chem. A.* **2017**, *5*, 19323–19332.
[37] F. Sun, G. Wang, Y. Ding, C. Wang, B. Yuan, Y. Lin, *Adv. Energy Mater.* **2018**, *8*, 1800584.
[38] B. Sherino, S. Mohamad, S. N. A. Halim, N. S. A. Manan, *Sens. Actuators B* **2018**, *254*, 1148–1156.
[39] H. Du, X. Zhang, Z. Liu, F. Qu, *Chem. Commun.* **2019**, *55*, 9653–9656.
[40] F. K. Saidu, A. Joseph, E. V. Varghese, G. V. Thomas, *Polym. Bull.* **2019**, 1–22.
[41] L. Wang, T. Wu, H. Wu, J. Zhong, N. Wang, R. Wang, *Prog. Nat. Sci-Mater.* **2018**, *28*, 24–27.
[42] A. Keziban, M. Özacar, *Mater. Chem. Phys.* **2021**, 124527.
[43] K. Dhara, D. R. Mahapatra, *J. Mater. Sci.* **2019**, *54*, 12319–12357.
[44] A. Ngamaroonchote, Y. Sanguansap, T. Wutikhun, K. Karnorachai, *Microchim. Acta.* **2020**, *187*, 1–12.
[45] C. Wang, S. Huang, L. Luo, Y. Zhou, X. Lu, G. Zhang, H. Ye, J. Gu, F. Cao, *J. Electroanal. Chem.* **2019**, *835*, 178–185.
[46] J. Li, Y. Liu, X. Tang, L. Xu, L. Min, Y. Xue, Z. Yang, *Mikrochim. Acta.* **2020**, *187*, 1–9.
[47] Y. Dong, J. Zheng, *Sens. Actuators B* **2020**, *311*, 127918.
[48] C. Duan, J. Zheng, *J. Electrochenm. Soc.* **2019**, *166*, B942.

Received: May 14, 2021
Accepted: May 28, 2021
Published online on ■■, ■■

RESEARCH ARTICLE

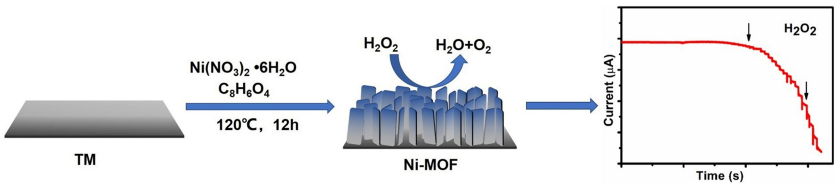

X. Liu, M.-H. Xiang, X. Zhang, Q. Li, X. Liu, W. Zhang, X. Qin, F. Qu**